

# THE ROLE OF ICE COMPOSITIONS AND MORPHOLOGY FOR SNOWLINES AND THE C/N/O RATIOS IN ACTIVE DISKS

ANA-MARIA A. PISO<sup>1</sup>, KARIN I. ÖBERG<sup>1</sup>, JAMILA PEGUES<sup>2</sup>

*Draft version March 7, 2016*

## ABSTRACT

The elemental compositions of planets define their chemistry, and could potentially be used as beacons for their formation location if the elemental gas and grain ratios of planet birth environments, i.e. protoplanetary disks, are well understood. In disks, the ratios of volatile elements, such as C/O and N/O, are regulated by the abundance of the main C, N, O carriers, their ice binding environment, and the presence of snowlines of major volatiles at different distances from the central star. We explore the effects of dynamical processes, molecular compositions and abundances, and the ice morphology of dust grains in disks on the snowline locations of the main C, O and N carriers, and their consequences for the C/N/O ratios in gas and dust throughout the disk. The gas-phase N/O ratio enhancement in the outer disk (exterior to the H<sub>2</sub>O snowline) exceeds the C/O ratio enhancement for all reasonable volatile compositions. Ice morphology and disk dynamics individually change the snowline location of N<sub>2</sub>, the main nitrogen carrier, by a factor of 2-3, and when considered together the range of possible N<sub>2</sub> snowline locations is  $\sim 11\text{--}79$  AU in a standard disk model. The CO snowline location is similarly uncertain. This snowline location uncertainty limits the utility of C/N/O compositional ratios in planets to trace their formation zone. Observations that anchor snowline locations at different stages of planet formation are therefore key.

## 1. INTRODUCTION

The chemical composition of protoplanetary disks is largely dictated by the freeze-out of volatile species. The snowline locations of volatile molecules are therefore crucial in determining disk chemical abundances in gas and dust, as well as planet compositions.

Carbon and oxygen bearing molecules, such as H<sub>2</sub>O, CO<sub>2</sub> and CO, as well as the carbon-to-oxygen (C/O) ratio in protoplanetary disks and in giant planet atmospheres have been extensively studied from a theoretical standpoint (Öberg et al. 2011b, Ali-Dib et al. 2014, Madhusudhan et al. 2014, Mollière et al. 2015), and snowlines of volatiles such as H<sub>2</sub>O and CO have been detected (Zhang et al. 2013, Qi et al. 2013). However, disk chemistry involves many other molecular compounds (Henning & Semenov 2013) including nitrogen bearing species and hydrocarbons (e.g., Mandell et al. 2012), which may affect the compositions of nascent planets.

Both in Solar system comets and in protoplanetary disks carbon and oxygen are primarily contained in H<sub>2</sub>O, CO<sub>2</sub> and CO (e.g., Lodders 2003, Mumma & Charnley 2011, Öberg et al. 2011b, Boogert et al. 2015). However, some fraction of the carbon abundance may also be carried by CH<sub>4</sub> (e.g., Öberg et al. 2008), which may change the C/O ratio in gas and in dust throughout the disk. In the case of nitrogen, chemical models of the protostellar nebula (e.g., Owen et al. 2001) and of protoplanetary disks (e.g., Rodgers & Charnley 2002) suggest that N<sub>2</sub> was the dominant form of nitrogen, and that giant planets have accreted their nitrogen content primarily as N<sub>2</sub> (Mousis et al. 2014). Observations of Solar system bodies such as Titan and Pluto show that N<sub>2</sub> is

prevalent in their atmospheres (Cruikshank et al. 1993, Owen et al. 1993). Moreover, the Rosetta spacecraft has recently made the first direct measurement of the N<sub>2</sub> abundance in comet 67P/Churyumov-Gerasimenko (Rubin et al. 2015). In addition to N<sub>2</sub>, a fraction of the nitrogen abundances may be also carried by NH<sub>3</sub> (Bottinelli et al. 2010, Mumma & Charnley 2011). Because of the high volatility of N<sub>2</sub>, the gas phase nitrogen-to-oxygen (N/O) ratio in the outer disk may be even more enhanced than the C/O ratio compared to its average value in the disk. Giant planets that form at wide separations should thus have an excess of nitrogen in their atmospheres, which could be used to trace their formation origin.

Moreover, snowline locations strongly depend on the ice grain morphology. Very volatile species, such as CO and N<sub>2</sub>, present binding energies, and therefore snowline locations, that are sensitive to the details of the morphology of the icy grain mantles. Laboratory experiments (Collings et al. 2003, Öberg et al. 2005, Bisschop et al. 2006, Fayolle et al. 2016) have shown that CO and N<sub>2</sub> have significantly different binding energies depending on whether they are pure or water dominated ices. This implies that ices in different environments will sublimate at different radii, which will substantially change the disk regions where these volatiles are present in gaseous or solid form (see Section 3.2).

In this work, we expand the coupled drift-desorption model developed in Piso et al. (2015) (hereafter Paper I) by considering additional volatile molecules and abundances, ice morphology, as well as nitrogen-to-oxygen (N/O) ratios.

This paper is organized as follows. In Section 2, we review the drift-desorption model developed in Paper I. We discuss the effect of different abundances of the main carbon, oxygen and nitrogen carriers, grain morphology

<sup>1</sup> Harvard-Smithsonian Center for Astrophysics, 60 Garden Street, Cambridge, MA 02138

<sup>2</sup> Department of Astrophysical Sciences, Princeton University

and disk dynamics on snowline locations and the C/N/O ratios in Section 3. We address the implications of our results in Section 4 and summarize our findings in Section 5.

## 2. COUPLED DRIFT-DESORPTION MODEL

We begin with a brief review of Paper I’s model for the effect of radial drift and viscous gas accretion on volatile snowline locations. We review our disk model in Section 2.1, and summarize our numerical method and results in Section 2.2.

### 2.1. Disk Model

In this work we consider both a static and a viscous disk. The static disk is irradiated by the central star and does not experience redistribution of solids or radial movement of the nebular gas. To quantify the effects of radial drift and gas accretion, we use a viscous disk with a spatially and temporally constant mass flux,  $\dot{M}$ . The viscous disk takes into account radial drift, gas accretion onto the central star, as well as accretion heating. We focus on this disk model which includes all the dynamical and thermal processes we are interested in for the scope of this paper, and do not further consider the other disk models presented in Paper I.

Following Chiang & Youdin (2010), the temperature profile for a static disk is

$$T = 120 (r/\text{AU})^{-3/7} \text{ K}, \quad (1)$$

where  $r$  is the semimajor axis. We use the Shakura & Sunyaev (1973) steady-state disk solution to model the viscous disk. From Paper I, the viscous disk temperature profile is computed as

$$T^4 = \left[ \frac{1}{4r} \left( \frac{3G\kappa_0 \dot{M}^2 M_* \mu m_p \Omega_k}{\pi^2 \alpha k_B \sigma} \right)^{1/3} \right]^4 + T_{\text{irr}}^4, \quad (2)$$

where  $T_{\text{irr}} = T$  from Equation (1). Here  $G$  is the gravitational constant,  $\kappa_0 = 2 \times 10^{-6}$  is a dimensionless opacity coefficient,  $M_* = M_\odot$  is the mass of the central star,  $\mu = 2.35$  is the mean molecular weight of the nebular gas,  $m_p$  is the proton mass,  $\Omega_k = \sqrt{GM_\odot/r^3}$  is the Keplerian angular velocity,  $\alpha = 0.01$  is a dimensionless coefficient (see below for details),  $k_B$  is the Boltzmann constant, and  $\sigma$  is the Stefan-Boltzmann constant.

The steady-state disk has an  $\alpha$ -viscosity prescription, where the kinematic viscosity is  $\nu = \alpha cH$ . Here  $c \equiv \sqrt{k_B T / (\mu m_p)}$  is the isothermal sound speed (with  $T$  from Equation 2), and  $H \equiv c/\Omega_k$  is the disk scale height. We can then determine the gas surface density for a viscous disk as (Shakura & Sunyaev 1973; see also Paper I for a more detailed explanation of these calculations):

$$\Sigma = \frac{\dot{M}}{3\pi\nu}. \quad (3)$$

We choose  $\dot{M} = 10^{-8} M_\odot \text{ yr}^{-1}$ , consistent with mass flux observations in disks (e.g., Andrews et al. 2010). As described in Paper I, the mass flux rate  $\dot{M}$  and stellar luminosity  $L_*$  will vary throughout the disk lifetime (Kennedy et al. 2006, Chambers 2009), in contrast with our simplified model which assumes that both quantities are constant. This effect will be most pronounced

in the inner disk ( $\lesssim$  few AU), where accretion heating dominates. We thus acknowledge that the location of the  $\text{H}_2\text{O}$  snowline may be determined by the decline in  $\dot{M}$  or  $L_*$  with time, rather than radial drift (see Paper I, Section 2.1 for a more detailed explanation).

### 2.2. Desorption-Drift Equations and Results

The model is described in full in Paper I, here we review and summarize key concepts and results. For a range of initial icy grain sizes composed of a single volatile, we showed in Paper I that the timescale on which these particles desorb is comparable to their radial drift time, as well as to the accretion timescale of the nebular gas onto the central star. We thus have to take into account both drift and gas accretion when we calculate the disk location at which a particle desorbs, since that location may be different from the snowline position in a static disk for a given volatile (see Figure 1 and Öberg et al. 2011b). We determine a particle’s final location in the disk by solving the following coupled differential equations:

$$\frac{ds}{dt} = -\frac{3\mu_x m_p}{\rho_s} N_x R_{\text{des},x} \quad (4a)$$

$$\frac{dr}{dt} = \dot{r}, \quad (4b)$$

where  $s$  is the particle size,  $t$  is time,  $\mu_x$  is the mean molecular weight of volatile  $x$ ,  $\rho_s = 2 \text{ g cm}^{-3}$  is the density of an icy particle,  $N_x \approx 10^{15} \text{ sites cm}^{-2}$  is the number of adsorption sites of molecule  $x$  per  $\text{cm}^{-2}$ ,  $R_{\text{des},x}$  is the desorption rate of species  $x$ , and  $\dot{r}$  is the particle’s radial drift velocity. We calculate  $R_{\text{des}}$  and  $\dot{r}$  as follows.

The desorption rate  $R_{\text{des},x}$  (per molecule) is (Hollenbach et al. 2009)

$$R_{\text{des},x} = \nu_x \exp(-E_x/T_{\text{grain}}), \quad (5)$$

where  $E_x$  is the adsorption binding energy in units of Kelvin,  $T_{\text{grain}} = T$  is the grain temperature (assumed to be the same as the disk temperature, see Paper I), and  $\nu_x = 1.6 \times 10^{11} \sqrt{(E_x/\mu_x)} \text{ s}^{-1}$  is the molecule’s vibrational frequency in the surface potential well. We discuss our choices for  $E_x$  for the different volatile species in Section 3.1.

Following Chiang & Youdin (2010) and Birnstiel et al. (2012), a particle’s radial drift velocity can be approximated as

$$\dot{r} \approx -2\eta\Omega_k r \left( \frac{\tau_s}{1 + \tau_s^2} \right) + \frac{\dot{r}_{\text{gas}}}{1 + \tau_s^2}, \quad (6)$$

where the first term is the drift velocity in a non-accreting disk and the second term accounts for the radial movement of the gas. Here  $\eta \approx c^2/(2v_k^2)$ , where  $v_k$  is the Keplerian velocity, and  $\tau_s \equiv \Omega_k t_s$  is the dimensionless stopping time:

$$t_s = \begin{cases} \rho_s s / (\rho c), & s < 9\lambda/4 \text{ Epstein drag} \\ 4\rho_s s^2 / (9\rho c \lambda), & s < 9\lambda/4, \text{ Re} \lesssim 1 \text{ Stokes drag,} \end{cases} \quad (7)$$

where  $\rho$  is the disk mid-plane density,  $\lambda$  is the mean free path and  $\text{Re}$  is the Reynolds number. The gas accretion velocity  $\dot{r}_{\text{gas}}$  is determined from  $\dot{M} = -2\pi r \dot{r}_{\text{gas}} \Sigma$ , for a fixed  $\dot{M}$  and with  $\Sigma$  given by Equation (3).

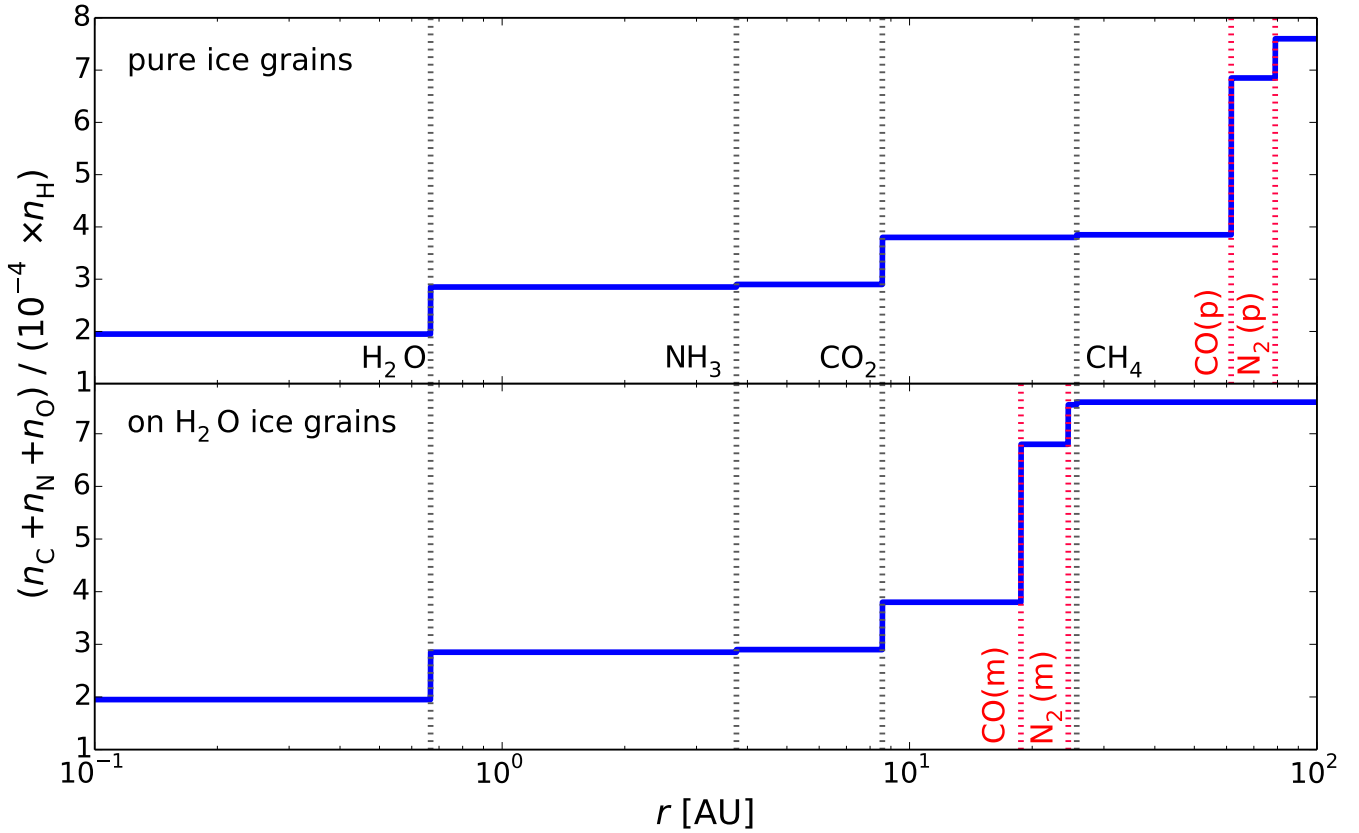


FIG. 1.— The total carbon, nitrogen and oxygen abundance as a function of semimajor axis in a static disk, for CO and N<sub>2</sub> as pure ices (top panel) and water dominated ices (bottom panel). Relevant volatile snowlines are marked by the vertical dashed lines. The grain abundances are calculated as a function of the observed median CH<sub>4</sub> and NH<sub>3</sub> abundances in protostellar cores. The total grain abundance increases with semimajor axis as more and more species freeze out.

For a particle of initial size  $s_0$ , we solve the Equation set (4) with the initial conditions  $s(t_0) = s_0$  and  $r(t_0) = r_0$ , where  $t_0$  is the time at which we start the integration and  $r_0$  is the particle's initial location. We stop our simulation after  $t_d = 3$  Myr, the disk lifetime, since this is roughly the timescale on which planets form, and determine the desorption timescale  $t_{\text{des}}$  from  $s(t_{\text{des}}) = 0$ , and thus a particle's desorption distance  $r_{\text{des}} = r(t_{\text{des}})$ . Our results are insensitive to our choice of  $t_0$  as long as  $t_0 \ll t_d$ . We note that a particle's size is initially fixed and only changes due to desorption. We thus do not take into account processes such as grain coagulation or fragmentation, which nonetheless occur in disks (e.g., Birnstiel et al. 2012, Pérez et al. 2012). We discuss the effect of these processes on snowline locations in Paper I.

As we show in Paper I, a particle of initial size  $s_0$  can experience three outcomes after  $t_d = 3$  Myr: (1) it can remain at its initial location, (2) it can drift towards the host star, then stop without evaporating significantly, and (3) it can completely desorb on a timescale shorter than 3 Myr. Particles in scenarios (1) and (2) are thus not affected by radial drift or gas accretion, and the snowline locations are those for a static disk. In contrast, the grains in case (3) desorb practically *instantaneously* and *at a fixed particle-size dependent location* in the disk, regardless of their initial position. The snowline locations for these particles will thus be fixed for a given initial

particle size and disk model. We have found that grains with sizes  $\sim 0.001 \text{ cm} \lesssim s \lesssim 7 \text{ m}$  satisfy this condition for our fiducial disk.

### 3. RESULTS

#### 3.1. Snowlines in a Static Disk: The Importance of Ice Morphology

As we note in Section 1, the disk volatile composition and the ice morphology determine the location of several important snowlines. In this work we focus on the primary carbon, oxygen and nitrogen carriers, i.e. H<sub>2</sub>O, CO<sub>2</sub>, CO, N<sub>2</sub>, and to a lesser extent, CH<sub>4</sub> and NH<sub>3</sub>. To quantify the effect of the presence of some carbon in the form of CH<sub>4</sub> and of some nitrogen in the form of NH<sub>3</sub>, we use measured median CH<sub>4</sub> and NH<sub>3</sub> abundances in protostellar cores from the *Spitzer* c2d Legacy ice survey (Evans et al. 2003).

We determine the location of the H<sub>2</sub>O, CO<sub>2</sub>, CO, CH<sub>4</sub>, N<sub>2</sub> and NH<sub>3</sub> snowlines in our static disk by balancing desorption with readorption, following Hollenbach et al. (2009). The binding energies of H<sub>2</sub>O, CO<sub>2</sub>, CO, CH<sub>4</sub>, N<sub>2</sub> and NH<sub>3</sub> as pure ices are 5800 K, 2000 K, 834 K, 1300 K, 767 K and 2965 K, respectively (Fraser et al. 2001, Collings et al. 2004, Fayolle et al. 2016, Garrod & Herbst 2006, Martín-Doménech et al. 2014). For CO and N<sub>2</sub> as water dominated ices, the binding energies are 1388 K and 1266 K, respectively (Fayolle et al. 2016). Figure 1 shows the resulting snowline locations, with CO and N<sub>2</sub>

pure ices (top panel) and water dominated ices (bottom panel). The ordinate displays the total carbon, oxygen and nitrogen abundance in solids as a function of the hydrogen total abundance. As expected, the total grain abundance increases with semimajor axis, as more and more species sublime. Freeze-out at the  $\text{CO}_2$  and  $\text{CO}$  snowlines pulls more heavy elements into the grains than in the case of the  $\text{H}_2\text{O}$  snowline. More importantly, the  $\text{CO}$  and  $\text{N}_2$  snowlines move several tens of AU inward if the ices are water dominated rather than pure. This changes the chemical abundances both in gas and dust throughout the disk, directly affecting the compositions of nascent giant planets forming in situ.

### 3.2. C/N/O Ratios in Static Disks

In this section we determine the C/O and N/O ratios in gas and dust throughout our static disk, and the extent to which they are affected by the presence of  $\text{CH}_4$  and  $\text{NH}_3$ . Since here we are primarily interested in the magnitude of the C/N/O ratios rather than snowline locations (which have been discussed in Section 3.1), we assume for simplicity that  $\text{CO}$  and  $\text{N}_2$  are pure ices.

We explore the parameter space of possible  $\text{CH}_4$  abundances by assuming three different scenarios: (1) no  $\text{CH}_4$ , (2) the median  $\text{CH}_4$  observed abundance (hereafter  $\text{CH}_4\text{-mid}$ ), and (3) the maximum  $\text{CH}_4$  observed abundance (hereafter  $\text{CH}_4\text{-max}$ ). Thus  $n_{\text{CH}_4\text{-mid}} = 0.0555 \times n_{\text{H}_2\text{O}}$  (Öberg et al. 2011a) and  $n_{\text{CH}_4\text{-max}} = 0.13 \times n_{\text{H}_2\text{O}}$  (Öberg et al. 2008), where  $n_{\text{H}_2\text{O}}$  is the total  $\text{H}_2\text{O}$  abundance. Similarly to Paper I, we use the  $\text{H}_2\text{O}$ ,  $\text{CO}_2$  and  $\text{CO}$  abundances of Öberg et al. (2011b). Since the abundance of carbon grains is uncertain, we assume that all the carbon that is not in the form of  $\text{CH}_4$ ,  $\text{CO}$  and  $\text{CO}_2$  is in carbon grains, so that we reproduce the Solar C/O ratio (gas+dust) of 0.54.

Figure 2 shows the C/O ratio in gas and dust as a function of semimajor axis in a static disk: no  $\text{CH}_4$  (top panel),  $\text{CH}_4\text{-mid}$  (middle panel) and  $\text{CH}_4\text{-max}$  (bottom panel). As in Öberg et al. (2011b) and Paper I, a gaseous C/O ratio of unity can be achieved between the  $\text{CO}_2$  and  $\text{CO}$  snowlines, where oxygen gas is significantly depleted. The gas-phase C/O ratio may be further enhanced between the  $\text{CO}_2$  and  $\text{CH}_4$  snowlines due to the presence of additional carbon gas from  $\text{CH}_4$ . In this region, the C/O ratio increases by 3% for  $\text{CH}_4\text{-mid}$  and by 8% for  $\text{CH}_4\text{-max}$ , as displayed in the middle and bottom panels of Figure 2. Based on the range of observed  $\text{CH}_4$  protostellar abundances, its presence in the disk only modestly affects the C/O ratio.

We assume that the main nitrogen-bearing species are  $\text{N}_2$  and  $\text{NH}_3$ , since other volatiles that contain nitrogen have significantly lower abundances in comparison (e.g., Mumma & Charnley 2011). We use the measured total nitrogen abundance in the Solar system,  $n_{\text{N}} = 8 \times 10^{-5} n_{\text{H}}$  (Lodders 2003), where  $n_{\text{H}}$  is the hydrogen abundance in the disk midplane. Similarly to the case of  $\text{CH}_4$ , we explore the parameter space of possible  $\text{NH}_3$  abundances using data from the Spitzer c2d Legacy ice survey, as follows: (1) no  $\text{NH}_3$ , (2) the median  $\text{NH}_3$  observed abundance  $n_{\text{NH}_3\text{-mid}} = 0.055 \times n_{\text{H}_2\text{O}}$  (Öberg et al. 2011a), and (3) the maximum observed  $\text{NH}_3$  abundance  $n_{\text{NH}_3\text{-max}} = 0.15 \times n_{\text{H}_2\text{O}}$  (Bottinelli et al. 2010). In each case, the  $\text{N}_2$  abundance then simply follows as

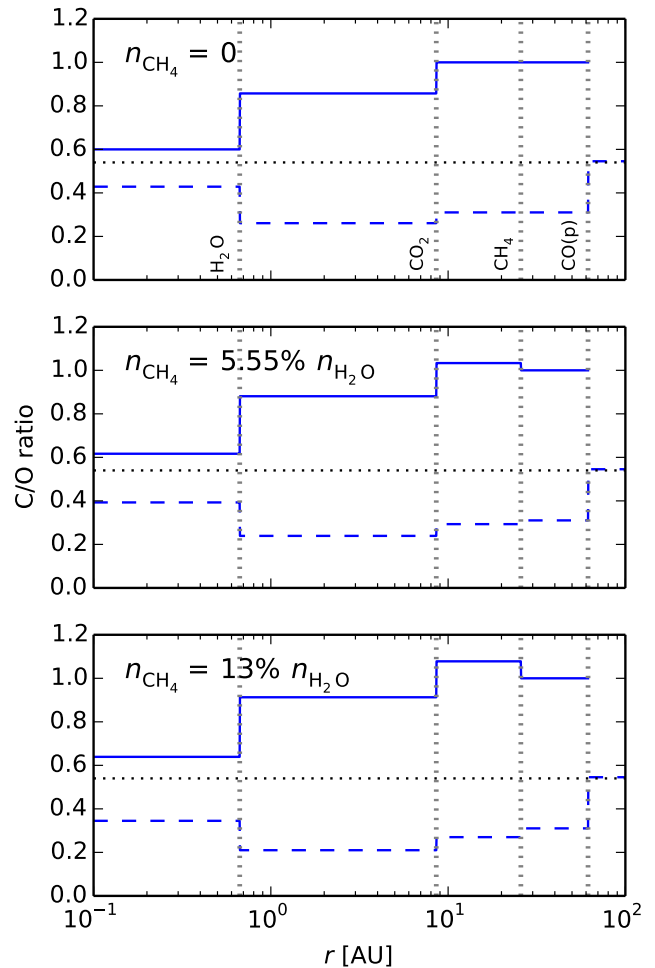


FIG. 2.— The C/O ratio in gas (solid lines) and dust (dashed lines) as a function of semimajor axis in a static disk, assuming no carbon is present in the form of  $\text{CH}_4$  (top panel), the median observed  $\text{CH}_4$  abundance is assumed (middle panel), and the maximum observed  $\text{CH}_4$  abundance is assumed (bottom panel). The C/O estimates are performed assuming that the  $\text{CO}$  ices are in pure form. The vertical dashed lines mark the snowline locations of the main C and O carriers. The horizontal dashed lines represent the stellar C/O value. The presence of methane only modestly increases the C/O ratio in gas between the  $\text{CO}_2$  and  $\text{CH}_4$  snowlines.

$$n_{\text{N}_2} = (n_{\text{N}} - n_{\text{NH}_3})/2.$$

Figure 3 shows the snowline locations of the main oxygen and nitrogen carriers and the N/O ratio in gas and dust as a function of semimajor axis in a static disk, for our three choices of the  $\text{NH}_3$  abundance: no  $\text{NH}_3$  (top panel),  $\text{NH}_3\text{-mid}$  (middle panel) and  $\text{NH}_3\text{-max}$  (bottom panel). For comparison, the horizontal dashed lines show the average N/O ratio in the disk. As expected, the gaseous N/O ratio generally exhibits an increasing trend towards the outer disk as more oxygen gas is depleted, with small decreases between the  $\text{NH}_3$  and  $\text{CO}_2$  snowlines (by 6% for  $\text{NH}_3\text{-mid}$  and by 18% for  $\text{NH}_3\text{-max}$ , respectively) due to  $\text{NH}_3$  freeze-out. While the presence of  $\text{NH}_3$  only moderately affects our results for the N/O ratio,  $\text{NH}_3$  is important since otherwise the nitrogen content in solid bodies would be more depleted than is observed for comets and asteroids (Wyckoff et al. 1991, Mumma & Charnley 2011, Bergin et al. 2015).

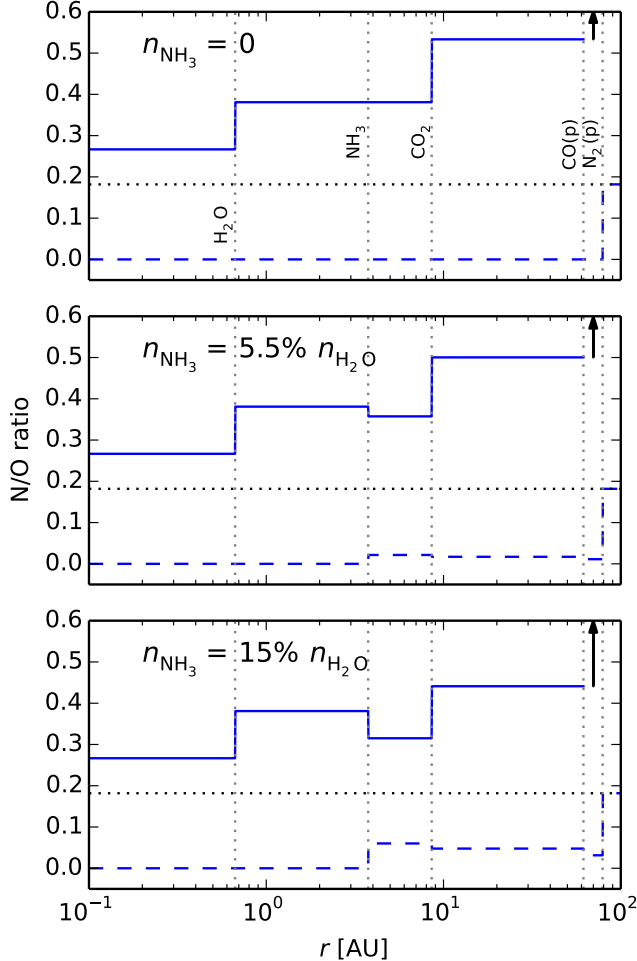


FIG. 3.— The N/O ratio in gas (solid lines) and dust (dashed lines) as a function of semimajor axis in a static disk, assuming no nitrogen is present in the form of  $\text{NH}_3$  (top panel), the median observed  $\text{NH}_3$  abundance is assumed (middle panel), and the maximum observed  $\text{NH}_3$  abundance is assumed (bottom panel). The N/O estimates are performed assuming that the CO and  $\text{N}_2$  ices are in pure form. The vertical dashed lines mark the snowline locations of the main C, O and N carriers. The horizontal dashed lines represent the average N/O value in the disk. The gas-phase N/O ratio is highly enhanced by a factor of three between the  $\text{CO}_2$  and CO snowlines compared to its average value. The arrows mark a highly elevated N/O ratio in gas between the CO and  $\text{N}_2$  snowlines due to the depletion of oxygen gas in this region. The presence of  $\text{NH}_3$  moderately decreases the N/O ratio in gas between the  $\text{NH}_3$  and  $\text{CO}_2$  snowlines.

The gas-phase N/O ratio is enhanced by a factor of two outside the  $\text{H}_2\text{O}$  snowline compared to its average value, by more than a factor of three between the  $\text{CO}_2$  and CO snowlines, and by orders of magnitude between the CO and  $\text{N}_2$  snowlines. This latter region can span tens of AU depending on disk parameters and the relative CO and  $\text{N}_2$  ice binding environment. This enhancement is more pronounced than the C/O gas phase enhancement of a factor of two in the outer disk (see Figure 2).

### 3.3. C/N/O Ratios in Dynamic Disks

Here we use the model of Section 2 to estimate the movement of the CO and  $\text{N}_2$  snowlines for different grain morphologies in a viscous disk. Figure 4 shows the  $\text{H}_2\text{O}$ ,

$\text{CO}_2$  and CO snowline locations for particles with initial sizes  $\sim 0.06 \text{ cm} \lesssim s \lesssim 7 \text{ m}$  as well as estimates for the C/O ratio in gas and dust in a viscous disk, with the CO snowline calculated under different grain morphologies as noted above. We assume there is no carbon in the form of  $\text{CH}_4$ . The true snowline for particles that desorb outside the static snowline is the static snowline itself, hence desorbing particles with  $s < 0.06 \text{ cm}$  do not form true snowlines. If the CO binding environment is known, the CO snowline moves inward by up to  $\sim 50\%$  compared to a static disk for each case (pure and water dominated ices) due to disk dynamics. The full range of potential CO snowlines taking into account both ice morphology and disk dynamics span  $\sim 8.7 \text{ AU}$  to  $\sim 61 \text{ AU}$ , which is a factor of  $\sim 7$  difference. This implies that gas phase C/O ratios of order unity may be reached in the giant planet forming zone, and the CO snowline may be inside 10 AU for certain disk parameters.

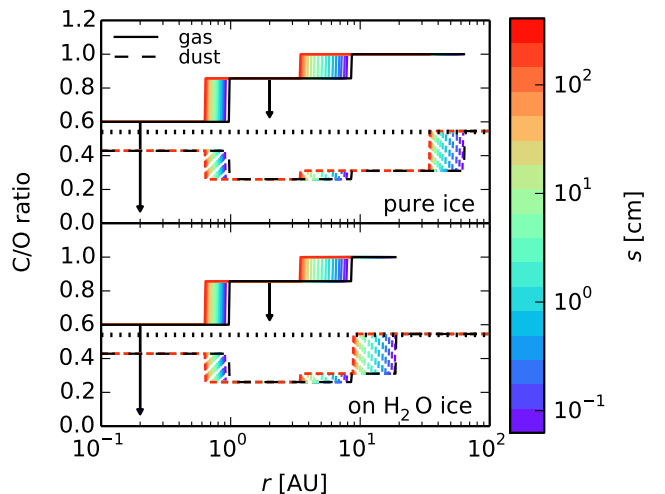


FIG. 4.— C/O ratio estimates in gas (solid lines) and dust (dashed lines) as function of semimajor axis in a viscous disk, for CO as pure ice (top panel) or as water dominated ices (bottom panel). The  $\text{H}_2\text{O}$ ,  $\text{CO}_2$  and CO snowlines are shown for particles with initial sizes  $\sim 0.001 \text{ cm} \lesssim s \lesssim 7 \text{ m}$  as indicated by the color bar. The C/O ratio in a static disk (black lines) is shown for comparison. The arrows show that the C/O ratio in gas will decrease inside the  $\text{H}_2\text{O}$  and  $\text{CO}_2$  snowlines in the viscous disk, as the relative fluxes of the desorbed icy particles and the overall nebular gas will cause an excess of oxygen gas inside these snowlines (see Paper I for details). The presence of CO in a water ice environment rather than as pure ice moves the CO snowline significantly inward by  $\sim 70\%$ . Taken together, disk dynamics and ice morphology move the CO snowline inward by a factor of  $\sim 7$ .

Figure 5 shows the  $\text{H}_2\text{O}$ ,  $\text{CO}_2$ , CO and  $\text{N}_2$  snowline locations in a viscous disk for the same range of initial particle sizes as in Figure 4, and with the CO and  $\text{N}_2$  snowlines calculated assuming different grain morphologies as explained above, as well as estimates for the N/O ratio throughout the disk. For simplicity, we assume that all nitrogen is bound in  $\text{N}_2$ . This choice is justified since the presence of some  $\text{NH}_3$  only moderately changes the N/O ratio (see Figure 3), and since we are primarily interested in the  $\text{N}_2$  snowline locations rather than exact values for the N/O ratio. The innermost  $\text{N}_2$  snowlines in the viscous disk, created by particles with  $s \sim 7 \text{ m}$  for our fiducial model, are located at  $r_{\text{N}_2, \text{pure}} \approx 42 \text{ AU}$



for  $N_2$  as pure ice and at  $r_{N_2, \text{water}} \approx 11$  AU for  $N_2$  in water dominated ices. Thus for each case (pure versus water dominated ices), the  $N_2$  snowline moves inward by up to 50% due to disk dynamics. By taking into account both ice morphology and disk dynamics, the full range of potential  $N_2$  snowlines span  $\sim 11$  to  $\sim 79$  AU, which is a factor of  $\sim 7$  difference. Similarly to the case for CO, the  $N_2$  snowline may be close to 10 AU for certain disk models.

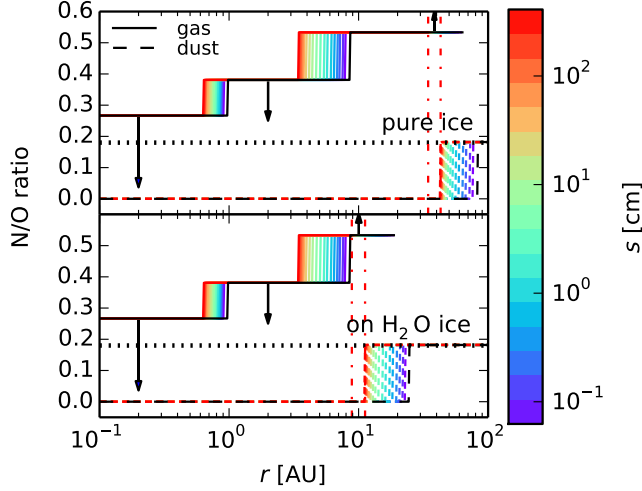


FIG. 5.— N/O ratio estimates in gas (solid lines) and dust (dashed lines) as function of semimajor axis in a viscous disk, for CO and  $N_2$  as pure ices (top panel) or as water dominated ices (bottom panel). The  $H_2O$ ,  $CO_2$  and  $N_2$  snowlines are shown for particles with initial sizes  $\sim 0.001 \text{ cm} \lesssim s \lesssim 7 \text{ m}$  as indicated by the color bar. The CO snowline (inner vertical dashed line in both panels) is only shown for the 7 m particles. The N/O ratio in a static disk (black lines) is shown for comparison. The downward arrows show that the N/O ratio in gas will decrease inside the  $H_2O$  and  $CO_2$  snowlines in the viscous disk, as the relative fluxes of the desorbed icy particles and the overall nebular gas will cause an excess of oxygen gas inside these snowlines (see Paper I for details). Radial drift and gas accretion move the  $N_2$  snowline inward by up to  $\sim 50\%$  compared to a static disk. The presence of  $N_2$  in a water ice environment rather than as pure ice moves the  $N_2$  snowline significantly inward by  $\sim 70\%$ . Taken together, disk dynamics and ice morphology move the CO snowline inward by a factor of  $\sim 7$ . The results of highly enhanced gas-phase N/O ratios between the  $CO_2$  and CO snowlines compared to its average value, and of highly elevated N/O ratios in gas between the CO and  $N_2$  snowlines (see Figure 3), are preserved.

#### 4. DISCUSSION

This study shows that the gas-phase N/O ratio in protoplanetary disks is considerably enhanced throughout most of the disk midplane compared to its average value. As demonstrated in Figure 6, the gaseous N/O ratio is enhanced by a factor of two beyond the  $H_2O$  snowline, by more than a factor of three between the  $CO_2$  and CO snowlines, and by several orders of magnitude between the CO and  $N_2$  snowlines. Thus constraining the N/O ratio in a giant planet atmosphere could be used to trace its formation origins. Theoretical models of the magnitude and role of N/O (and N/C) ratios in exoplanet atmospheres are therefore key in order to use these ratios as probes for a planet’s formation location. Measurements of the N/O ratio in planet atmospheres are essential to

further constrain the theoretical expectations — while nitrogen-bearing molecules have not been targeted so far due to lack of instrument sensitivity, such observations and detections are likely in the near future with the advent of JWST (e.g.,  $NH_3$ , Greene et al. 2016).

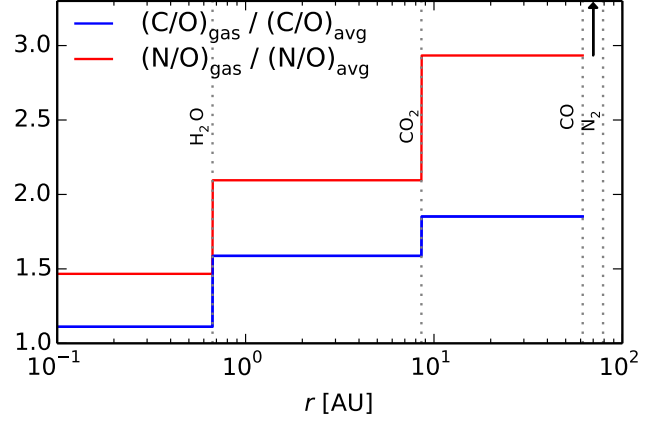


FIG. 6.— Gas phase C/O (blue curve) and N/O (red curve) ratios divided by the average C/O and N/O ratio in the disk, assuming CO and  $N_2$  are pure ices, and there is no  $CH_4$  or  $NH_3$ . The dashed vertical lines mark the  $H_2O$ ,  $CO_2$ , CO and  $N_2$  snowlines. The arrow indicates that the N/O ratio is enhanced by orders of magnitude compared to its average value between the CO and  $N_2$  snowlines. The gaseous N/O ratio is enhanced throughout most of the disk, and more enhanced than the C/O ratio.

The N/O ratio enhancement is larger than that of the gas phase C/O ratio throughout most of the disk. Thus measurements of an enhanced C/O ratio in an exoplanet atmosphere could be corroborated (disproved) by measurements of enhanced (non-enhanced) N/O ratios. Moreover, Figure 6 shows that giant planets that have formed in situ between the  $H_2O$  and CO snowlines are expected to present elevated both C/O and N/O ratios in their atmospheres, whereas planets between the CO and  $N_2$  snowlines will have a highly enhanced N/O ratio in their atmospheres, but not C/O.

Due to disk dynamics and ice morphology, the disk regions with highly elevated gas phase N/O and C/O ratios are uncertain and may span tens of AU. In particular, one can imagine a scenario where CO is in a water binding environment and  $N_2$  is not. This could be attributed to the fact that  $H_2O$  may bind preferentially to CO than  $N_2$ , since both  $H_2O$  and CO are polar molecules while  $N_2$  is not. It is also possible for  $N_2$  ices to form later than CO (e.g., Pagani et al. 2012), and thus be deposited on the outer layers of the icy mantles which are typically water poor (e.g., Garrod & Pauly 2011). Detections of CO and  $N_2$  snowlines in the same disk could potentially verify this scenario, since CO and  $N_2$  desorb at substantially different temperature, and therefore locations, if the former is water dominated and the latter is in a pure ice environment. Changes in stellar luminosity (e.g., Kennedy et al. 2006) and gas mass accretion rate (e.g., Chambers 2009) may introduce additional uncertainties in the snowline locations, and thus the C/N/O ratios (see also Paper I). The impact of the ice environment on the snowline location is much smaller in the case of  $CO_2$  and  $NH_3$ , as their binding energies and behavior

are closer to that of  $\text{H}_2\text{O}$ . No detailed measurements for the  $\text{CH}_4$  binding energy in a water environment exist so far, but due to its low desorption temperature a similar behavior to that of  $\text{CO}$  and  $\text{N}_2$  would be expected. While the presence of some carbon in the form of  $\text{CH}_4$  only modestly affects our results,  $\text{CH}_4$  may become important in disks where a large fraction of the  $\text{CO}$  abundance has been converted into hydrocarbons (e.g., Du et al. 2015).

Our results could also be applied to the Solar system. Recent measurements of nitrogen abundance in comet 67P/Churyumov-Gerasimenko found a  $\text{N}_2/\text{CO}$  ratio  $\sim 10^{-3}$  (Rubin et al. 2015). A low  $\text{N}_2/\text{CO}$  ratio is consistent with comets having formed inside the  $\text{N}_2$  snowline where solid  $\text{N}_2$  is depleted. Theoretical models suggest that Jupiter-family comets, such as 67P, originate from the Kuiper belt (Duncan & Levison 1997) (but see Rubin et al. 2015 for alternative formation scenarios for 67P). It is thus possible, in principle, to use measurements of the  $\text{N}_2$  abundance in Jupiter-family comets to determine where the  $\text{N}_2$  snowline was located in our Solar system. However due to the uncertainty in the calculated location of the  $\text{N}_2$  snowline (see Section 3.3), more detailed modeling is needed.

Finally, detections of snowlines in disks that are reasonably well characterized could help further constrain the dynamics and ice morphology in the disks.

## 5. SUMMARY

In this paper we explore the role of icy grain morphology and disk dynamics on the snowline locations of major volatile carrier molecules and the C/N/O ratios in protoplanetary disks. We enhance the coupled drift-desorption model developed in Piso et al. (2015) by adding more carbon- and nitrogen-bearing species into our framework and by considering different binding ice environments. Our results can be summarized as follows:

1. Due to the high volatility of  $\text{N}_2$ , the gaseous N/O ratio outside the  $\text{H}_2\text{O}$  snowline is enhanced by a factor of two compared to its average value, by more than a factor of three between the  $\text{CO}_2$  and  $\text{CO}$  snowlines, and by many orders of magnitude between the  $\text{CO}$  and  $\text{N}_2$  snowlines due to the com-

plete depletion of oxygen gas in this region. This enhancement is more pronounced than in the case of the gas-phase C/O ratio, which is increased by at most a factor of two compared to the stellar value.

2. The presence of some carbon in the form of  $\text{CH}_4$  only modestly affects our results for the gas phase C/O ratio, increasing it by up to 8% between the  $\text{CO}_2$  and  $\text{CH}_4$  snowlines. The presence of some nitrogen in the form of  $\text{NH}_3$  moderately affects our results and may decrease the gaseous N/O ratio by up to 18% between the  $\text{NH}_3$  and  $\text{CO}_2$  snowlines. In both cases, large gas phase C/O and N/O ratios in the outer disk are preserved.
3. Grain composition sensitively affects the  $\text{CO}$  and  $\text{N}_2$  snowline locations. If  $\text{CO}$  and  $\text{N}_2$  are water dominated rather than pure ices, their snowlines move inward by up to  $\sim 70\%$ . This effect is separate from that of radial drift and viscous gas accretion, which also cause an inward movement of the  $\text{CO}$  and  $\text{N}_2$  snowlines by up to  $\sim 50\%$ .
4. The locations of the  $\text{CO}$  and  $\text{N}_2$  snowlines are uncertain when we consider both viscous versus static disks, and pure versus water dominated ices. The snowlines in a viscous disk with  $\text{CO}$  or  $\text{N}_2$  in a water environment are by up to a factor of  $\sim 7$  closer to the host star than in a static disk with  $\text{CO}$  or  $\text{N}_2$  as pure ices.

Our results have direct consequences for the composition of nascent giant planets. The considerable inward movement of the  $\text{CO}$  and  $\text{N}_2$  snowlines due to the ice grains being water dominated rather than pure ices implies that giant planets with high C/O and/or N/O ratios in their atmospheres may form closer in than previously predicted by theoretical models. Moreover, our model shows that wide separation gas giants may have an excess of nitrogen in their envelopes, which may be used to trace their origins. In future work, we plan to add new levels of complexity to our model in terms of disk chemistry, dynamics, and planetary dynamics, thus forming a solid framework for understanding the origins of gas giants.

## REFERENCES

- Ali-Dib, M., Mousis, O., Petit, J.-M., & Lunine, J. I. 2014, *ApJ*, 785, 125
- Andrews, S. M., Wilner, D. J., Hughes, A. M., Qi, C., & Dullemond, C. P. 2010, *ApJ*, 723, 1241
- Bergin, E. A., Blake, G. A., Ciesla, F., Hirschmann, M. M., & Li, J. 2015, *Proceedings of the National Academy of Science*, 112, 8965
- Birnstiel, T., Klahr, H., & Ercolano, B. 2012, *A&A*, 539, A148
- Bisschop, S. E., Fraser, H. J., Öberg, K. I., van Dishoeck, E. F., & Schlemmer, S. 2006, *A&A*, 449, 1297
- Boogert, A. C. A., Gerakines, P. A., & Whittet, D. C. B. 2015, *ARA&A*, 53, 541
- Bottinelli, S., Boogert, A. C. A., Bouwman, J., et al. 2010, *ApJ*, 718, 1100
- Chambers, J. E. 2009, *ApJ*, 705, 1206
- Chiang, E., & Youdin, A. N. 2010, *Annual Review of Earth and Planetary Sciences*, 38, 493
- Collings, M. P., Anderson, M. A., Chen, R., et al. 2004, *MNRAS*, 354, 1133
- Collings, M. P., Dever, J. W., Fraser, H. J., & McCoustra, M. R. S. 2003, *Ap&SS*, 285, 633
- Cruikshank, D. P., Roush, T. L., Owen, T. C., et al. 1993, *Science*, 261, 742
- Du, F., Bergin, E. A., & Hogerheijde, M. R. 2015, *ArXiv e-prints*, arXiv:1506.03510
- Duncan, M. J., & Levison, H. F. 1997, *Science*, 276, 1670
- Evans, II, N. J., Allen, L. E., Blake, G. A., et al. 2003, *PASP*, 115, 965
- Fayolle, E. C., Balfe, J., Loomis, R., et al. 2016, *ApJ*, 816, L28
- Fraser, H. J., Collings, M. P., McCoustra, M. R. S., & Williams, D. A. 2001, *MNRAS*, 327, 1165
- Garrod, R. T., & Herbst, E. 2006, *A&A*, 457, 927
- Garrod, R. T., & Pauly, T. 2011, *ApJ*, 735, 15
- Greene, T. P., Line, M. R., Montero, C., et al. 2016, *ApJ*, 817, 17
- Henning, T., & Semenov, D. 2013, *Chemical Reviews*, 113, 9016
- Hollenbach, D., Kaufman, M. J., Bergin, E. A., & Melnick, G. J. 2009, *ApJ*, 690, 1497
- Kennedy, G. M., Kenyon, S. J., & Bromley, B. C. 2006, *ApJ*, 650, L139
- Lodders, K. 2003, *ApJ*, 591, 1220
- Madhusudhan, N., Amin, M. A., & Kennedy, G. M. 2014, *ApJ*, 794, L12
- Mandell, A. M., Bast, J., van Dishoeck, E. F., et al. 2012, *ApJ*, 747, 92
- Martín-Doménech, R., Muñoz Caro, G. M., Bueno, J., & Goesmann, F. 2014, *A&A*, 564, A8

- Mollière, P., van Boekel, R., Dullemond, C., Henning, T., & Mordasini, C. 2015, *ApJ*, 813, 47
- Mousis, O., Fletcher, L. N., Lebreton, J.-P., et al. 2014, *Planet. Space Sci.*, 104, 29
- Mumma, M. J., & Charnley, S. B. 2011, *ARA&A*, 49, 471
- Öberg, K. I., Boogert, A. C. A., Pontoppidan, K. M., et al. 2008, *ApJ*, 678, 1032
- . 2011a, *ApJ*, 740, 109
- Öberg, K. I., Murray-Clay, R., & Bergin, E. A. 2011b, *ApJ*, 743, L16
- Öberg, K. I., van Broekhuizen, F., Fraser, H. J., et al. 2005, *ApJ*, 621, L33
- Owen, T., Mahaffy, P. R., Niemann, H. B., Atreya, S., & Wong, M. 2001, *ApJ*, 553, L77
- Owen, T. C., Roush, T. L., Cruikshank, D. P., et al. 1993, *Science*, 261, 745
- Pagani, L., Bourgoïn, A., & Lique, F. 2012, *A&A*, 548, L4
- Pérez, L. M., Carpenter, J. M., Chandler, C. J., et al. 2012, *ApJ*, 760, L17
- Piso, A.-M. A., Öberg, K. I., Birnstiel, T., & Murray-Clay, R. A. 2015, *ApJ*, 815, 109
- Qi, C., Öberg, K. I., Wilner, D. J., et al. 2013, *Science*, 341, 630
- Rodgers, S. D., & Charnley, S. B. 2002, *MNRAS*, 330, 660
- Rubin, M., Altwegg, K., Balsiger, H., et al. 2015, *Science*, 348, 232
- Shakura, N. I., & Sunyaev, R. A. 1973, *A&A*, 24, 337
- Wyckoff, S., Tegler, S. C., & Engel, L. 1991, *ApJ*, 367, 641
- Zhang, K., Pontoppidan, K. M., Salyk, C., & Blake, G. A. 2013, *ApJ*, 766, 82